Available online at www.sciencedirect.com
SCIENCE DIRECT
Remote Sensing of Environment 103 (2006) 97–114
Remote Sensing of Environment
www.elsevier.com/locate/rse

Tree cover and height estimation in the Fennoscandian tundra–taiga transition zone using multiangular MISR data

Janne Heiskanen *

Department of Geography, University of Helsinki, P.O. Box 64, FI-00014, University of Helsinki, Finland

Received 3 November 2005; received in revised form 28 March 2006; accepted 31 March 2006

Abstract

The tundra–taiga transition zone stretches around the northern hemisphere separating boreal forest to the south from treeless tundra to the north. Tree cover and height are important variables to characterize this vegetation transition. Accurate continuous fields of tree cover and height would enable the delineation of the forest extent according to different criterion and provide useful data for change detection of this climatically sensitive ecotone. This study examined if multiangular remote sensing data has potential to improve the accuracy of the tree cover and height estimates in relation to nadir-view data. The satellite data consisted of Multi-angle Imaging SpectroRadiometer (MISR) data at 275 m and 1.1 km resolutions. The study area was located in the Fennoscandian tundra–taiga transition zone, in northernmost Finland. The continuous fields of tree cover and height were estimated using neural networks, which were trained and assessed by high-resolution biotope inventory data. The spectral–angular data together produced lower estimation errors than single band nadir, multispectral nadir or single band multiangular data alone. RMSE of the tree cover estimates reduced from 7.8% (relative RMSE 67.4%) to 6.5% (56.1%) at 275 m resolution, and from 5.4% (49.2%) to 4.1% (36.9%) at 1.1 km resolution, when multispectral nadir data were used together with multiangular data. RMSE of the tree height estimates reduced from 2.3 m (44.3%) to 2.0 m (37.6%) and from 1.8 m (35.4%) to 1.3 m (25.4%), respectively. The largest estimation errors occurred in mires and in areas of dense shrub cover, but the use of multiangular data also reduced estimation errors in these areas. The results suggest that directional information has potential to improve the tree cover and height estimates, and hence the accuracy of the land cover change detection in the tundra–taiga transition zone.

Keywords: Multiangular; MISR; Tundra–taiga transition zone; Tree cover; Tree height; Neural networks

1. Introduction

The tundra–taiga interface stretches around the northern hemisphere separating boreal forest to the south from treeless tundra to the north (Callaghan et al., 2002b). Instead of a clearly defined forest line, it is a transition zone characterized by latitudinal gradients of tree cover, density, height, age-class structure and growth form. These gradients are associated with gradients in climate, biodiversity, land–atmosphere interaction, snow dynamics, and land use. Locally, the gradients are modified by topography and, for example, by the presence of rivers and mires (Callaghan et al., 2002b). If global warming and climate change continue as predicted, they are likely to have a major impact on vegetation distribution and structure in the tundra–taiga transition zone (Skre et al., 2002). This will have significant effects on ecosystem functioning and biodiversity, and also possible feedback effects on climate (Harding et al., 2002). The response of vegetation cover to the climate change is likely to show local variability depending on the local environmental conditions (Skre et al., 2002). Forest fires, insect outbreaks and human activities, like reindeer herding, industry and land use changes, make the land cover change even more complex (Käyhkö & Pellikka, 1994; Seppälä & Rastas, 1980; Skre et al., 2002; Vlassova, 2002).

Standardised and more precise land cover characterization in the tundra–taiga boundary is necessary for monitoring

* Tel.: +358 9 19150770.
E-mail address: janne.heiskanen@helsinki.fi.

0034-4257/$ - see front matter © 2006 Elsevier Inc. All rights reserved.
doi:10.1016/j.rse.2006.03.015

natural and human induced land cover changes in the future (Callaghan et al., 2002a,b). Remote sensing offers probably the only cost-effective means for monitoring the regional variability in land cover change over the vast tundra–taiga transition zone (Rees et al., 2002; Stow et al., 2004). Wide-swath, low spatial resolution instruments like NOAA AVHRR, Terra/Aqua MODIS and SPOT VEGETATION provide data that allow land cover characterization over the whole transition zone regularly, for example, annually. Relatively large parts of the transition zone have also been covered by high resolution image mosaics, for example, by Landsat TM images (e.g., Virtanen et al., 2004). However, high temporal resolution is essential, if regular monitoring is pursued in the high latitudes, where data acquisition is hindered by frequent cloud cover and the short growing season (Rees et al., 2002; Stow et al., 2004). High spatial resolution airborne and spaceborne instruments enable more detailed but less frequent analyses of land cover change, and calibration and validation of lower resolution observations (Stow et al., 2004).

The tundra–taiga transition zone has been mapped in several global and continental scale land cover classifications at 1 km spatial resolution (Bartalev et al., 2003; Bartholomé & Belward, 2005; Hansen et al., 2000; Loveland et al., 2000). In conventional land cover maps, every pixel is labelled to a single land cover type. The classification of low resolution pixels to a single land cover type generally results in an underestimation of the less abundant and more fragmented land cover classes (Braswell et al., 2003; Virtanen et al., 2004). The internal heterogeneity of discrete classes is also obscured (DeFries et al., 2000a, 2000b). An alternative is to map the sub-pixel fractions of different land cover classes, or to describe land cover as continuous fields (e.g., Fernandes et al., 2004). This means either mapping the proportional covers of land cover types, or estimation of surfaces of land cover describing variables (e.g., percent tree cover). In principle, these approaches provide methods for detecting spatial gradients and temporal changes in land cover, and methods for unbiased estimation of land cover over large areas with low spatial resolution sensors (DeFries et al., 2000a; Fernandes et al., 2004). Continuous fields of land cover attributes are also independent of different classification legends (DeFries et al., 2000b). A number of methods exist for deriving sub-pixel land cover, for example, linear spectral unmixing, regression analysis and neural networks (Boyd et al., 2002; Fernandes et al., 2004; Hansen et al., 2003; Schwarz & Zimmermann, 2005).

The tundra–taiga transition zone is characterized by the changing proportions of the tundra and taiga vegetation. However, apart from the global continuous fields of vegetation products (DeFries et al., 1999, 2000a, 2000b; Hansen et al., 2003), only a very few studies have used the sub-pixel methods to characterize the land cover of this ecotone. Tree cover and height have been used in the global land cover classification legends to define forest classes (e.g., Loveland et al., 2000). Accurately mapped continuous fields of the tree cover and tree height would enable the delineation of the forest extent according to variable criterion. It would also be desirable to map separately coniferous and broadleaved tree cover, because climate change may affect the tree species composition, and also because different species are likely to have a different response to climate change (Skre et al., 2002).

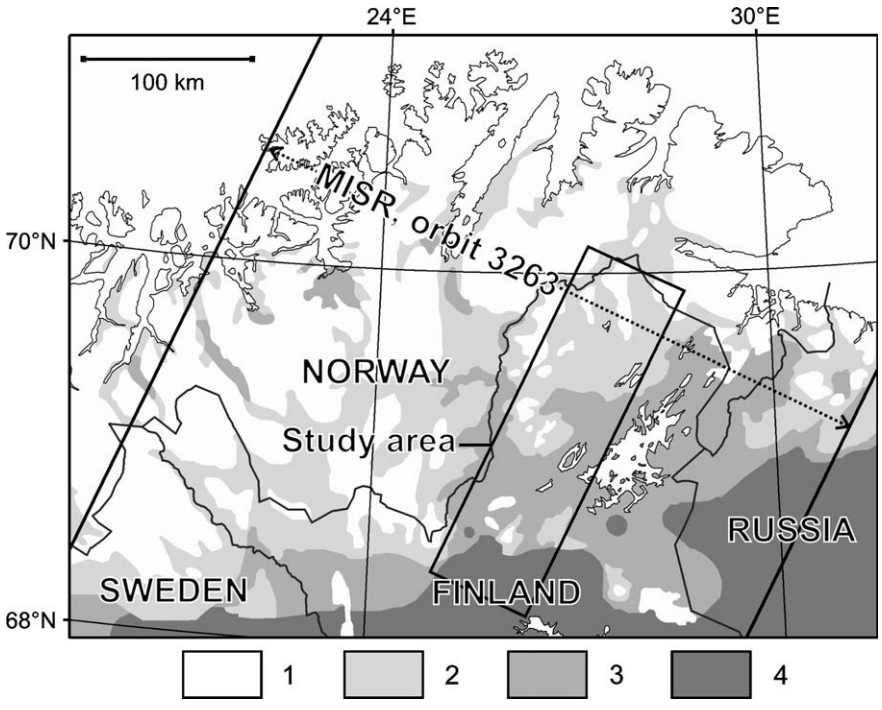

Fig. 1. The location of the study area and vegetation zones after Oksanen and Virtanen (1995): 1 = treeless heath, 2 = birch woodland and forest, 3 = pine forest and 4 = mixed coniferous forest. The map also shows the width of the MISR orbit.

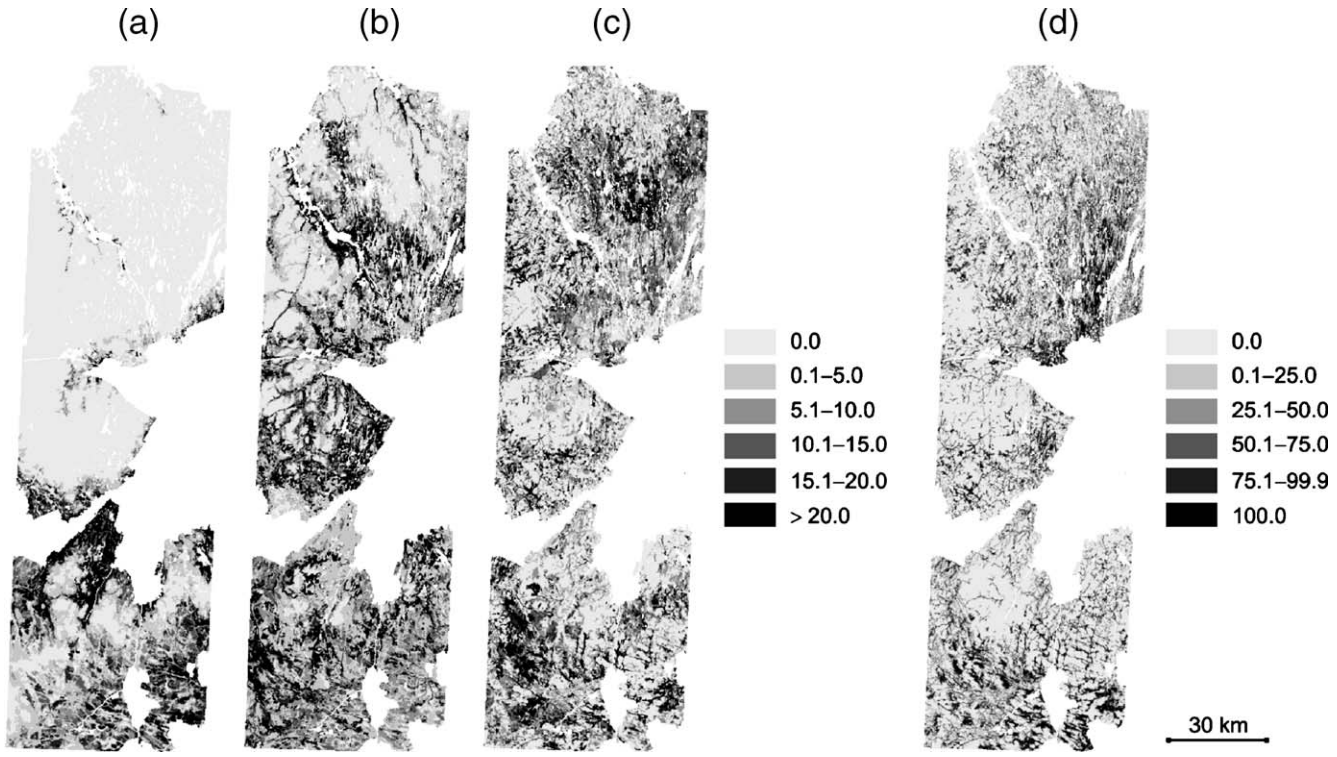

Fig. 2. (a) The spatial variability of coniferous tree cover (%), (b) broadleaved tree cover (%), (c) shrub cover (%), and (d) fractional cover of mire (%) in the study area at 275 m resolution.

Significant differences have been observed between the global land cover maps in the transition zones of the major biomes (Hansen & Reed, 2000). Accurate mapping of the tundra–taiga transition zone has been hampered by the spectral confusion between forest and non-forest vegetation (Rees et al., 2002). The effect of the undergrowth vegetation on the satellite signal is also pronounced in areas of low tree cover (DeFries et al., 2000b). In the higher resolution studies, the classification errors have occurred typically in the sparse forests and heaths with particularly dense undergrowth shrub cover (Käyhkö & Pellikka, 1994; Seppälä & Rastas, 1980; Virtanen et al., 2004). Also mires, which are abundant in the tundra–taiga transition zone, are often misinterpreted as forest (Häme et al., 1997; Kalliola & Syrjänen, 1991; Tomppo et al., 2002). These sources of error are likely to reduce the classification accuracy and bias the continuous fields estimates in the tundra–taiga transition zone.

Bidirectional reflectance distribution function (BRDF) describes the dependence of the satellite observed reflectance on solar illumination and sensor viewing angles. BRDF of vegetation is typically highly anisotropic, determined by the optical properties of canopy components, and canopy- and landscape-level structural characteristics (Asner et al., 1998). Most of the remote sensing studies concerned with land cover mapping have employed the spectral and temporal information of the optical satellite data. However, several studies (Abuelgasim et al., 1996; Barnsley et al., 1997; Bicheron et al., 1997; Diner et al., 1999) have suggested that directional information gathered by the multiangular sensors (i.e. sensors with multiple view angles) could separate land cover types with similar spectral reflectances at nadir. The significant variability in structural properties of vegetation in the tundra–taiga transition zone implies that multiangular data could potentially increase the accuracy of land cover mapping in this transition zone. Recently, near-simultaneous multiangular observations have also become available, providing improved sampling of land surface BRDF (Asner et al., 1998; Diner et al., 1998).

The objective of this study was to examine the potential of multiangular remote sensing data to improve the continuous fields of tree cover and height estimates in the tundra–taiga transition zone in northernmost Finland. The remote sensing data consisted of Multi-angle Imaging SpectroRadiometer (MISR) data at 275 m and 1.1 km spatial resolutions. MISR data was employed to examine the sensitivity of multiangular reflectance to the variability in tree cover and height, and to study how the accuracy of the tree cover and height estimates depends on the utilized spectral–angular band combination. The estimation accuracy was also studied in relation to the shrub cover and fractional cover of mire.

2. Material and methods

2.1. Study area

The study area was a 215-km-long and 60-km-wide transect located in the Fennoscandian tundra–taiga transition zone, in northernmost Finland (Fig. 1). The study area belongs to the northern boreal and hemiarctic vegetation zones (Heikkinen, 2005; Oksanen & Virtanen, 1995). The area lies south of the latitudinal tree line of mountain birch (*Betula pubescens* ssp.

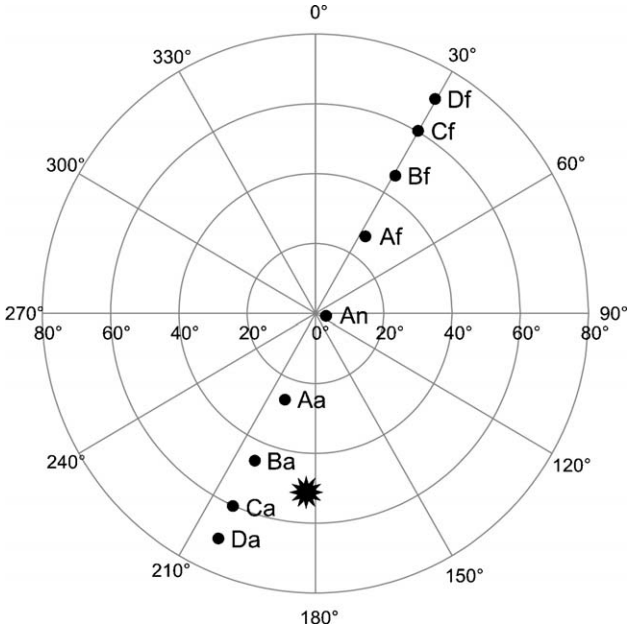

Fig. 3. A polar plot showing the mean viewing angles of the MISR cameras and Sun position during the data acquisition. The circular axis represents the azimuth angle and the radial axis represents the zenith angle.

czerepanovii), but the tree lines of Scots pine (*Pinus sylvestris*) and Norway spruce (*Picea abies*) transect the area (Heikkinen, 2005). The area north of the pine forests is characterized by treeless heaths, mountain birch woodlands and forests, and sporadic pine stands. The southern part is characterized by pine forests and mixed coniferous forests (Fig. 1). Palsa and orohemiarctic mires are typical in the northern part and aapa mires in the southern part of the study area (Ruuhijärvi, 1988). Dwarf birch (*B. nana*) is a common shrub not only in the undergrowth of mountain birch forests but also in the heaths and mires. The herbivorous larvae of the geometrid moth *Epirrita autumnata* have defoliated the mountain birch woodlands and forests over large areas from time to time (Seppälä & Rastas, 1980). The topography of the study area is characterised by gently sloping fells and steep slopes in the river valleys, and elevation ranges from approximately 100 to 600 m a.s.l.

2.2. Biotope inventory data

The biotopes of the nature reserves, wilderness areas and national parks of northernmost Finland have been inventoried between 1996 and 1999 (Sihvo, 2001, 2002). According to the definition, biotope is an area with uniform soil, tree stand and human impact (Eeronheimo, 1996). The biotope map has been delineated from colour-infrared aerial photographs using interpretation keys collected in the field. The basic forest inventory parameters have also been interpreted. The scale of the inventory was 1:20 000 and the smallest mapping unit 1 ha. The biotope data has been stored in a GIS-database in vector format. The tree cover and height were used as target variables. The tree cover has been defined as the projected cover of the predominant tree layer in percentage, and tree height as the mean of the hundred thickest trees in a hectare in metres (Eeronheimo, 1996). The coniferous and broadleaved tree covers were also derived by using the species-specific fractions of the total tree cover. The shrub cover, i.e. the projected coverage of shrubs in percentage (Eeronheimo, 1996), and mire and water masks were derived as ancillary data. A mire mask included all the mire biotopes.

The spatial variability of the coniferous and broadleaved tree cover, shrub cover and fractional cover of mire in the study area are presented in Fig. 2. The private lands have not been inventoried and hence the data did not cover the entire study area.

2.3. Satellite data

The multiangular satellite data were provided by MISR, which is onboard the Earth Observing System (EOS) satellite Terra (Diner et al., 1998, 2002). MISR has nine cameras; four

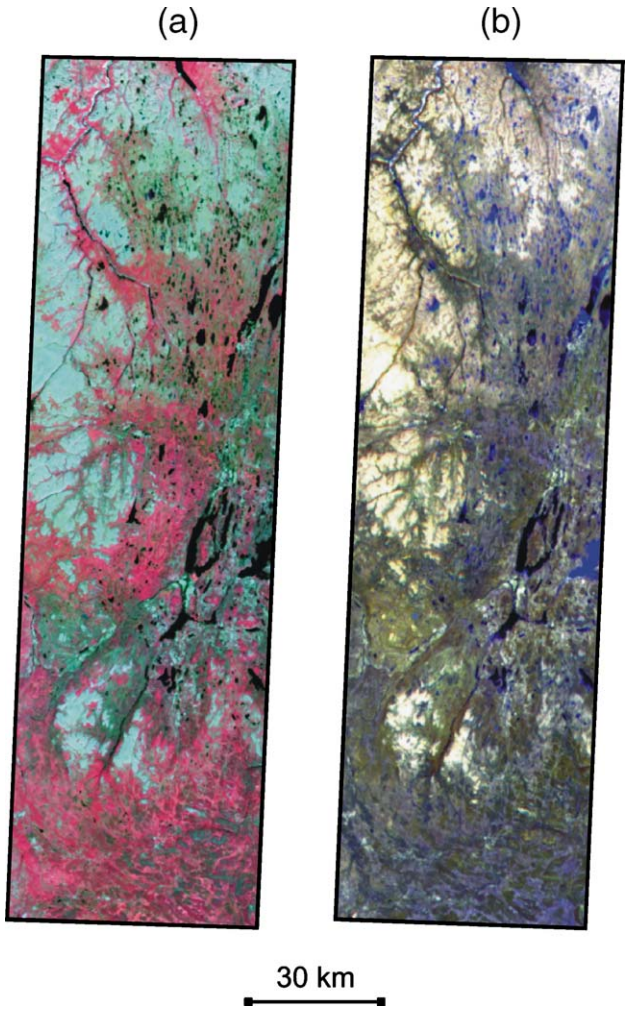

Fig. 4. Multispectral and -angular RGB composites of the MISR Level 1B2 Terrain data at 275 m resolution. Composites consist of NIR, red and green bands from nadir viewing camera (a) and red bands from 60° forward, nadir and 60° aftward viewing cameras (b). (For interpretation of the references to colour in this figure legend, the reader is referred to the web version of this article.)

Table 1
Descriptive statistics of the reference data at 275 m and 1.1 km resolution

Variable	Resolution	*n*	Range	Mean	Median	S.D.
Tree cover (%)	275 m	123 512	0.0–79.1	11.5	8.5	11.4
	1.1 km (TOA BRF)	6998	0.0–47.9	11.0	9.6	9.3
	1.1 km (surface BRF)	5760	0.0–47.9	11.6	10.8	9.6
Coniferous tree cover (%)	275 m	123 512	0.0–50.0	3.6	0.0	7.0
	1.1 km (TOA BRF)	6998	0.0–38.4	3.4	0.0	6.0
	1.1 km (surface BRF)	5760	0.0–38.4	4.0	0.0	6.3
Broadleaved tree cover (%)	275 m	123 512	0.0–76.8	7.7	4.4	9.0
	1.1 km (TOA BRF)	6998	0.0–46.6	7.4	5.9	6.8
	1.1 km (surface BRF)	5760	0.0–46.6	7.4	5.8	6.9
Tree height (m)	275 m	123 512	0.0–17.8	5.3	4.3	3.7
	1.1 km (TOA BRF)	6998	0.0–16.0	5.1	4.3	3.3
	1.1 km (surface BRF)	5760	0.0–16.0	5.4	4.4	3.5
Shrub cover (%)	275 m	123 512	0.0–100.0	6.7	3.7	8.2
	1.1 km (TOA BRF)	6998	0.0–51.7	6.7	5.3	6.0
	1.1 km (surface BRF)	5760	0.0–51.7	6.6	4.9	6.2
Fractional cover of mire (%)	275 m	123 512	0.0–100.0	21.2	6.6	28.2
	1.1 km (TOA BRF)	6998	0.0–100.0	21.2	16.1	19.4
	1.1 km (surface BRF)	5760	0.0–100.0	18.9	14.0	18.2

point to the forward direction (entitled Af, Bf, Cf, and Df in the order of increasing off-nadir angle), one points towards the nadir (An) and four point to the aftward direction (Aa, Ba, Ca, Da). The nominal view angles of the cameras are 0°, ±26.1°, ±45.6°, ±60.0° and ±70.5°. Each of the nine cameras has four spectral bands: blue (centered at 446 nm; bandwidth 42 nm), green (558 nm; 29 nm), red (672 nm; 22 nm) and near infrared (NIR, 866 nm; 40 nm) (Diner et al., 1998). MISR data are acquired at a spatial resolution of 275 m, but in the global mode the original resolution is preserved only for the red bands and nadir camera, the other bands being averaged to a 1.1 km resolution.

MISR data employed in this study were acquired on 29 July 2000 (path 193 and orbit 3263). The acquisition date corresponds approximately to the time of maximum birch leaf size in the study area. Defoliation of the birch leaves by *E. autumnata* is not known to have occurred in the study area in summer 2000. Fig. 3 shows the mean view zenith and azimuth angles of the MISR cameras during the data acquisition. The scattering angle, i.e. the angle between the illumination and observation directions defined by the zenith and azimuth angles, was the smallest for Ba and Ca cameras, 21° and 24°, respectively.

A set of standard MISR data products are available, ranging from the raw instrument data to the calibrated and geolocated radiances, and geophysical retrievals of atmospheric and surface properties (Bothwell et al., 2002). MISR Level 1B2 Terrain data [MI1B2T, terrain projected top-of-atmosphere (TOA) radiance] and MISR Level 2 Land Surface data [MIL2ASLS, surface bidirectional reflectance factor (BRF)] were used here. The Land Surface data is only available at 1.1 km resolution. The data were provided by the Atmospheric Sciences Data Center (ASDC) at NASA Langley Research Center and ordered from the EOS Data Gateway.[1] TOA radiances were converted into TOA BRFs using the exo-atmospheric irradiances, Earth–Sun distance and solar zenith angle accompanying the data.

Fig. 4 shows multispectral and -angular composites of MISR L1B2 Terrain imagery over the study area.

2.4. Compilation of the statistical data set

The spatial resolution of the MISR data determined that the target variables were estimated at 275 m and 1.1 km resolutions. All the biotope inventory data were rasterised to a 15 m resolution and projected to the Space Oblique Mercator (SOM) projection corresponding to the MISR data. Two grids were created matching the 275 m and 1.1 km MISR pixels. The mean tree cover (also separate coniferous and broadleaved tree cover) and tree height were calculated for the grid cells. Also, the mean shrub cover and fractional covers of water and mire were calculated. The cells that were not covered by the biotope inventory data completely, or that had a fractional cover of water over 30% were excluded.

The input variables included all the bands from the nadir camera and red bands from all the cameras at 275 m resolution (TOA BRF), and all the bands from all the cameras at 1.1 km resolution (TOA and surface BRF). However, the data from Da camera was not used due to the obvious errors in the co-registration with other cameras. For the other cameras, the mean geolocation error has been reported to be below 60 m (standard deviations ranging from 100 to 300 m) and coregistration of the cameras within one pixel uncertainty (Diner et al., 2002; Jovanovic et al., 2002). After the exclusion of Da camera, there were 11 bands at 275 m resolution, and 32 bands at 1.1 km resolution. Some pixels were excluded from the Level 1B2 Terrain data because they were obscured by topography in the extreme view angles (Jovanovic et al., 1998). The Level 2 Land Surface data have been atmospherically corrected using atmospheric parameters at 17.6×17.6 km^2 regions. Data were missing for some regions reducing the number of observations in surface BRF data set.

The descriptive statistics of the reference data at 275 m and 1.1 km resolution are shown in Table 1. The total number of pixels was 123 512 at 275 m resolution, and 6998 (TOA BRF) and 5760 (surface BRF) at 1.1 km resolution. Half of all the data were allocated to the training set and half to the testing set by random sampling.

[1] http://edcimswww.cr.usgs.gov/pub/imswelcome/.

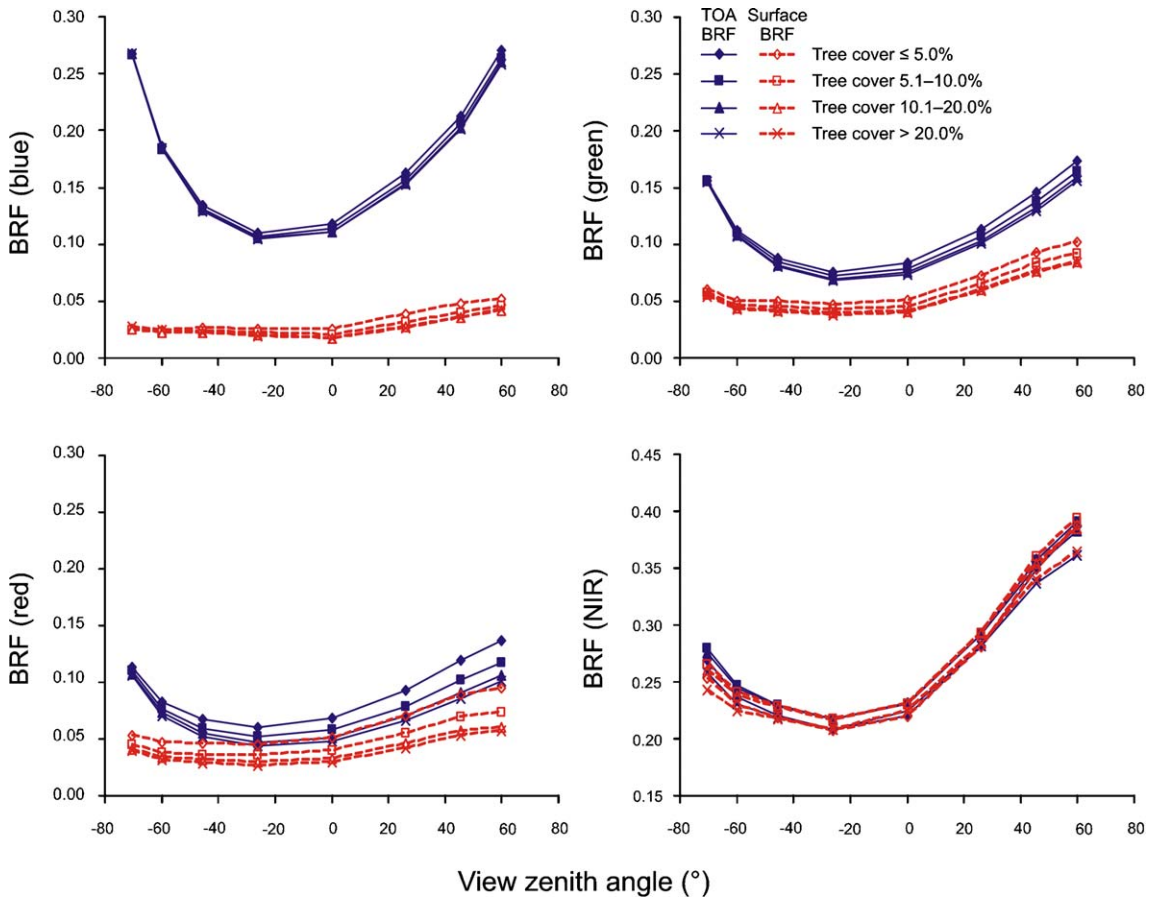

Fig. 5. The mean blue, green, red and NIR top-of-atmosphere (TOA) and surface BRF in the tree cover classes and MISR viewing angles (−70.5° to 60.0°). The negative angles correspond to the forward scatter direction (view azimuth 190°) and positive angles to the backward scattering direction (view azimuth 10°). The solar zenith angle was 51° at time of acquisition. (For interpretation of the references to colour in this figure legend, the reader is referred to the web version of this article.)

2.5. Data analysis

The mean TOA and surface BRFs were calculated for several tree cover and height classes before the statistical analysis. This was done in order to visualize the dependence of the BRFs on the view zenith angle, and tree cover and height in MISR spectral bands.

The tree cover and height were estimated by neural networks using different combinations of MISR bands. Neural networks are general-purpose computing tools that can solve complex nonlinear problems (Bishop, 1995). The major attraction of neural networks is that, unlike conventional statistical methods, they offer a powerful means for analysing complex data sets without making assumptions about the data distribution (Boyd et al., 2002). Therefore, neural networks have been used commonly for estimation of forest variables using remote sensing data (Boyd et al., 2002; Fernandes et al., 2004).

Feed-forward multilayer neural networks were applied in this study. Various architectures having one and two hidden layers with variable number of neurons (from 5 to 40 in steps of 5) were investigated separately for all the target variables. The models producing the most accurate estimates were selected. Hyperbolic tangent activation functions were used in the hidden nodes. The Network training was performed using the Levenberg–Marquardt algorithm (Bishop, 1995). Early stopping was adopted in order to avoid overfitting of the models (Bishop, 1995). The training set, i.e. 50% of all the observations, was partitioned randomly to the training data (90%) and to the validation data (10%), and the training was stopped at the point of minimum validation set error.

2.6. Model assessment

The trained networks were used in the forward mode to estimate the target variables for the testing data set. The reliability statistics included the root mean square error (RMSE), relative RMSE ($RMSE_r$), bias (Bias) and relative bias ($Bias_r$):

$$\mathrm{RMSE} = \sqrt{\frac{\sum_{i=1}^{n} (\hat{y}_i - y_i)^2}{n}} \quad (1)$$

$$\mathrm{RMSE_r} = \frac{\mathrm{RMSE}}{\bar{y}} \times 100 \quad (2)$$

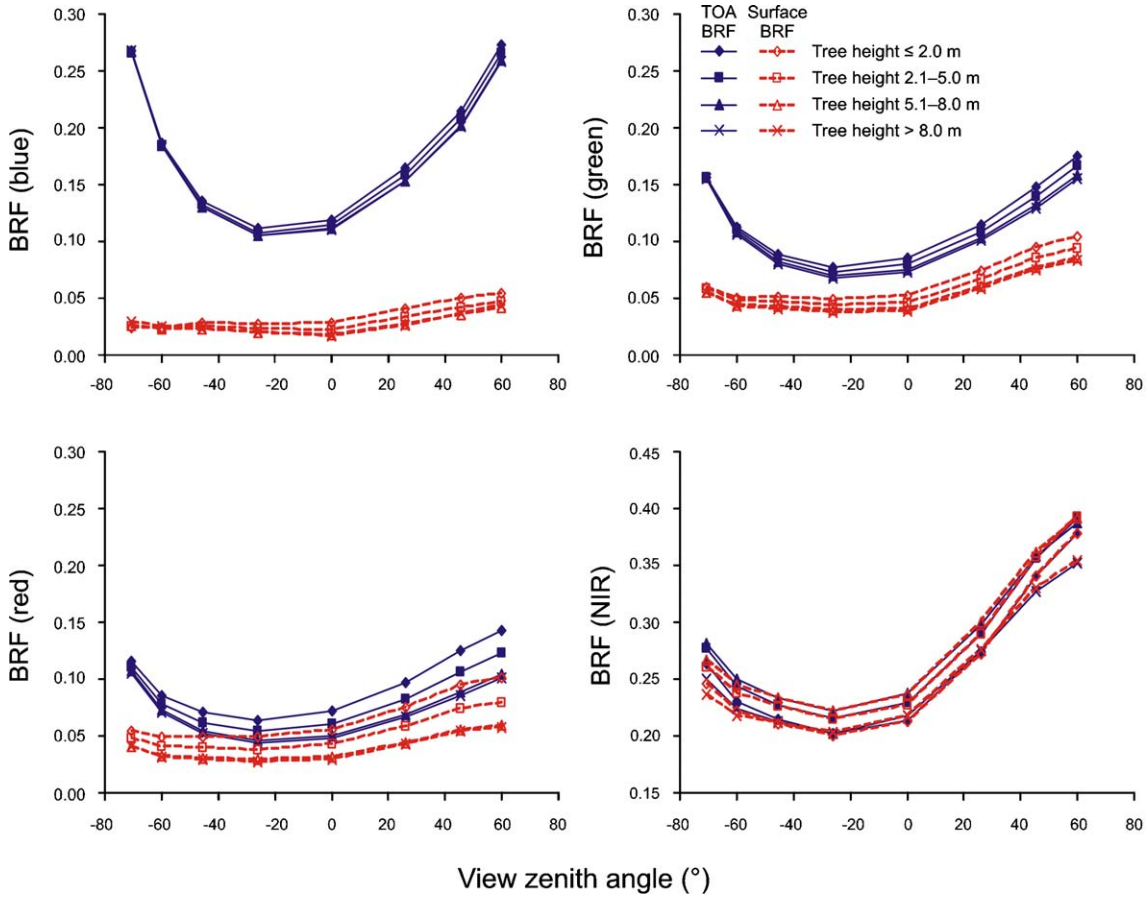

Fig. 6. The mean blue, green, red and NIR top-of-atmosphere (TOA) and surface BRF in the tree height classes and MISR viewing angles (−70.5° to 60.0°). See Fig. 5 for details. (For interpretation of the references to colour in this figure legend, the reader is referred to the web version of this article.)

$$\text{Bias} = \frac{\sum_{i=1}^{n} (\hat{y}_i - y_i)}{n} \quad (3)$$

$$\text{Bias}_r = \frac{\text{Bias}}{\bar{y}} \times 100 \quad (4)$$

where $\hat{y}_i$ is the estimate, y_i is the observed value, $\bar{y}$ is the mean of the observations and n is the number of the observations (Hyvönen, 2002). The statistical significance of the bias was tested using the t-test.

3. Results

3.1. BRF of tree cover and height classes

The mean TOA and surface BRFs differ considerably in the shorter wavelength blue, green and red bands but very little in the NIR bands (Figs. 5 and 6). The atmospheric correction reduces the BRF particularly in the largest off-nadir view angles. The TOA BRF increases rapidly with increasing view zenith angle, being higher in the backscatter direction than in the corresponding angles in the forward scatter direction. The surface BRFs are flattened, especially in the forward scatter direction. The BRF is lowest in 26.1° forward viewing camera and highest in 45.6° and 60.0° aftward viewing cameras, i.e. in the smallest scattering angles. The NIR bands show the largest range of surface BRF and also the strongest forward scatter. The forward scatter is also slightly increasing towards the extreme forward viewing direction.

The differences between the tree cover and height classes are approximately equal both in the TOA and surface BRF data. In the blue, green and red bands, the mean BRFs are systematically decreasing as tree cover and height increase. The differences between the tree cover classes are greatest in the backscatter direction in the red bands. The largest tree cover classes are distinguishable, but the two largest tree height classes have very similar BRFs in the red bands. The differences between the classes are particularly small in the blue and green bands. In the NIR bands, the highest and lowest tree cover and height classes have very similar BRFs. However, the largest three classes have clear differences.

3.2. Tree cover and height estimation

All the target variables were estimated by neural networks having one hidden layer. The number of hidden units in the

Table 2
The accuracy of the tree cover and height estimates at 275 m spatial resolution using different spectral–angular combinations of MISR bands (n=61 756)

Target variable	View-angle [a] (spectral band [b])	Number of bands	RMSE	$RMSE_r$ (%)	Bias	$Bias_r$ (%)	r
Tree cover (%)	Nadir (blue)	1	8.98	77.6	**−0.10**	−0.8	0.61
	Nadir (green)	1	9.24	79.9	**−0.09**	−0.8	0.58
	Nadir (red)	1	8.41	72.7	**−0.08**	−0.7	0.67
	Nadir (NIR)	1	11.15	96.4	**−0.09**	−0.8	0.20
	Nadir (all)	4	7.80	67.4	−0.11	−1.0	0.73
	All (red)	8	6.85	59.2	−0.03	−0.3	0.80
	Nadir (all), All (red)	11	6.49	56.1	−0.05	−0.4	0.82
Coniferous tree cover (%)	Nadir (blue)	1	6.45	178.3	0.01	0.4	0.37
	Nadir (green)	1	5.91	163.5	0.00	−0.1	0.52
	Nadir (red)	1	6.20	171.5	0.00	−0.1	0.45
	Nadir (NIR)	1	6.47	179.0	**−0.02**	−0.7	0.36
	Nadir (all)	4	4.71	130.4	**0.10**	2.8	0.73
	All (red)	8	4.91	135.6	**0.05**	1.3	0.71
	Nadir (all), All (red)	11	3.85	106.5	−0.02	−0.6	0.83
Broadleaved tree cover (%)	Nadir (blue)	1	7.98	103.4	**−0.10**	−1.3	0.47
	Nadir (green)	1	8.29	107.4	**−0.12**	−1.5	0.40
	Nadir (red)	1	7.90	102.3	**−0.10**	−1.2	0.49
	Nadir (NIR)	1	8.52	110.4	**−0.08**	−1.1	0.34
	Nadir (all)	4	7.18	93.0	−0.06	−0.7	0.61
	All (red)	8	6.87	89.0	**−0.09**	−1.2	0.65
	Nadir (all), All (red)	11	6.43	83.2	**−0.06**	−0.8	0.71
Tree height (m)	Nadir (blue)	1	2.99	56.9	0.01	0.3	0.57
	Nadir (green)	1	2.90	55.1	0.00	0.0	0.61
	Nadir (red)	1	2.81	53.3	0.00	0.0	0.64
	Nadir (NIR)	1	3.58	68.0	0.00	−0.1	0.19
	Nadir (all)	4	2.33	44.3	0.00	0.0	0.77
	All (red)	8	2.29	43.5	0.02	0.4	0.78
	Nadir (all), All (red)	11	1.98	37.6	0.01	0.2	0.84

Biases shown in bold are statistically significant (p<0.05). The table also shows correlations of the observed and estimated values (r).
[a] Nadir=An camera; all=Df, Cf, Bf, Af, An, Aa, Ba and Ca cameras.
[b] Blue=blue band; green=green band; red=red band; NIR=near infrared band; all=blue, green, red and NIR bands.

hidden layer varied from 10 to 35. The number of hidden units increased as the number of input bands increased. Less than 100 iterations were necessary to train all the networks.

The accuracy statistics of the tree cover and height estimates at 275 m resolution are presented in Table 2. The multispectral nadir bands and multiangular red data together produced consistently the smallest estimation errors and the highest correlations between the observed and predicted values. The smallest RMSE was 6.49% for tree cover and 1.98 m for tree height. $RMSE_r$ were smaller for tree height than for tree cover, the smallest errors being 37.6% and 56.1%, respectively. The division of tree cover into coniferous and broadleaved tree cover decreased RMSE but increased $RMSE_r$ considerably. The smallest RMSE ($RMSE_r$) was 3.85% (106.5%) for coniferous and 6.43% (83.2%) for broadleaved tree cover. The biases of the most accurate tree cover and height estimates were small and insignificant. Some of the coniferous and broadleaved tree cover estimates had larger and significant biases.

The surface BRF data produced consistently lower accuracy for all the target variables than TOA BRF data. This is most probably due to a quilted pattern in the surface BRF data, which

Table 3
The accuracy of the tree cover and height estimates at 1.1 km spatial resolution using different spectral–angular combinations of MISR bands (n=3499)

Variable	View-angle [a] (spectral band [b])	Number of bands	RMSE	$RMSE_r$ (%)	Bias	$Bias_r$ (%)	r
Tree cover (%)	Nadir (blue)	1	6.63	60.1	0.02	0.2	0.69
	Nadir (green)	1	7.17	65.0	−0.06	−0.5	0.63
	Nadir (red)	1	6.07	55.0	0.07	0.6	0.75
	Nadir (NIR)	1	8.87	80.5	**0.08**	0.7	0.27
	Nadir (all)	4	5.42	49.2	−0.14	−1.3	0.81
	All (blue)	8	5.74	52.0	**−0.26**	−2.4	0.78
	All (green)	8	5.21	47.2	−0.09	−0.8	0.83
	All (red)	8	4.62	41.9	0.05	0.4	0.87
	All (NIR)	8	5.80	52.6	−0.21	−1.9	0.78
	Nadir (all), All (red)	11	4.27	38.7	−0.07	−0.6	0.89
	All (all)	32	4.06	36.9	−0.11	−1.0	0.90
Coniferous tree cover (%)	Nadir (blue)	1	5.22	161.1	**0.17**	5.4	0.42
	Nadir (green)	1	4.87	150.5	**0.12**	3.7	0.53
	Nadir (red)	1	4.93	152.2	**0.27**	8.3	0.52
	Nadir (NIR)	1	5.48	169.1	**0.20**	6.2	0.31
	Nadir (all)	4	3.59	110.9	0.09	2.8	0.78
	All (blue)	8	4.29	132.5	0.14	4.4	0.67
	All (green)	8	3.42	105.7	**0.25**	7.7	0.81
	All (red)	8	3.82	118.0	**0.27**	8.3	0.75
	All (NIR)	8	3.10	95.7	−0.04	−1.2	0.84
	Nadir (all), All (red)	11	2.55	78.8	0.06	1.8	0.90
	All (all)	32	2.23	68.9	0.07	2.3	0.92
Broadleaved tree cover (%)	Nadir (blue)	1	5.73	76.1	**−0.25**	−3.3	0.56
	Nadir (green)	1	6.04	80.2	**−0.19**	−2.6	0.48
	Nadir (red)	1	5.69	75.5	**−0.28**	−3.8	0.57
	Nadir (NIR)	1	6.13	81.3	**−0.15**	−1.9	0.46
	Nadir (all)	4	4.86	64.6	−0.08	−1.0	0.71
	All (blue)	8	5.38	71.4	**−0.19**	−2.5	0.63
	All (green)	8	5.25	69.6	**−0.18**	−2.4	0.65
	All (red)	8	4.81	63.9	**−0.24**	−3.2	0.72
	All (NIR)	8	5.33	70.7	**−0.26**	−3.4	0.64
	Nadir (all), All (red)	11	4.45	59.1	**−0.16**	−2.2	0.76
	All (all)	32	3.96	52.5	−0.10	−1.3	0.82
Tree height (m)	Nadir (blue)	1	2.50	49.1	0.05	1.1	0.62
	Nadir (green)	1	2.51	49.3	0.00	0.0	0.62
	Nadir (red)	1	2.28	44.7	0.03	0.6	0.70
	Nadir (NIR)	1	3.16	61.9	**0.08**	1.7	0.17
	Nadir (all)	4	1.80	35.4	−0.02	−0.4	0.83
	All (blue)	8	1.96	38.5	0.01	0.1	0.79
	All (green)	8	1.74	34.1	0.00	−0.1	0.84
	All (red)	8	1.80	35.2	0.06	1.2	0.83
	All (NIR)	8	1.81	35.6	−0.07	−1.3	0.83
	Nadir (all), All (red)	11	1.40	27.5	0.00	0.1	0.90
	All (all)	32	1.29	25.4	−0.01	−0.2	0.91

The variables were estimated by TOA BRF data. Biases shown in bold are statistically significant (p<0.05). The table also shows correlations of the observed and estimated values (r).
[a] Nadir=An camera; all=Df, Cf, Bf, Af, An, Aa, Ba and Ca cameras.
[b] Blue=blue band; green=green band; red=red band; NIR=near infrared band; all=blue, green, red and NIR bands.

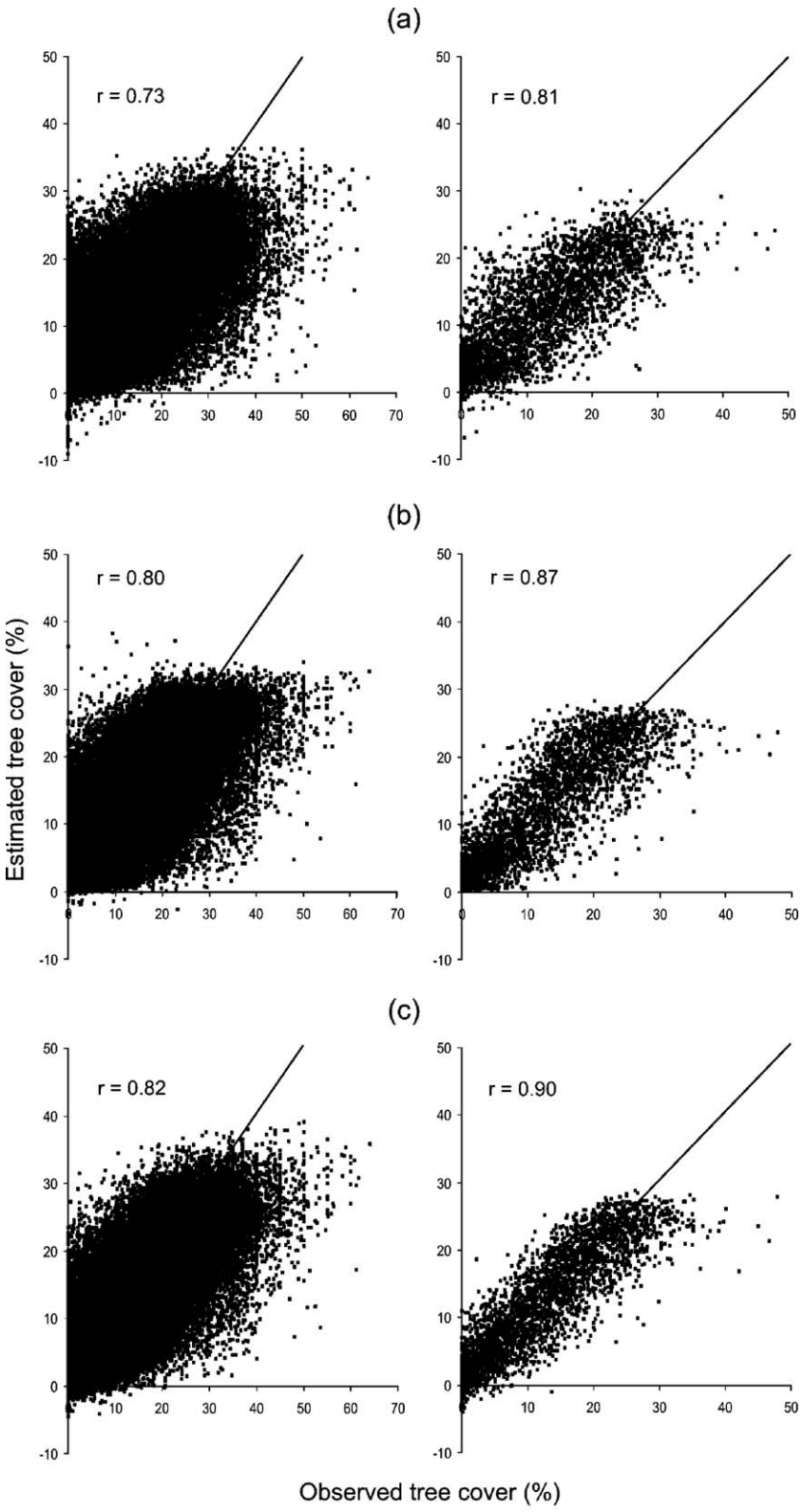

Fig. 7. Estimated versus observed tree cover (%) at 275 m resolution (on the left) and at 1.1 km resolution (on the right). Input variables included all nadir bands (a), multiangular red bands (b) and all the bands (c).

is a result of 17.6×17.6 km^2 regions used in the atmospheric correction (Diner et al., 2005). Because of artefacts in surface BRF data, the accuracy statistics are presented only for the TOA data (Table 3).

The tree cover and height estimates were more accurate at 1.1 km resolution than at 275 m resolution. The smallest estimation errors and the highest correlation between the observed and predicted values were observed when all the

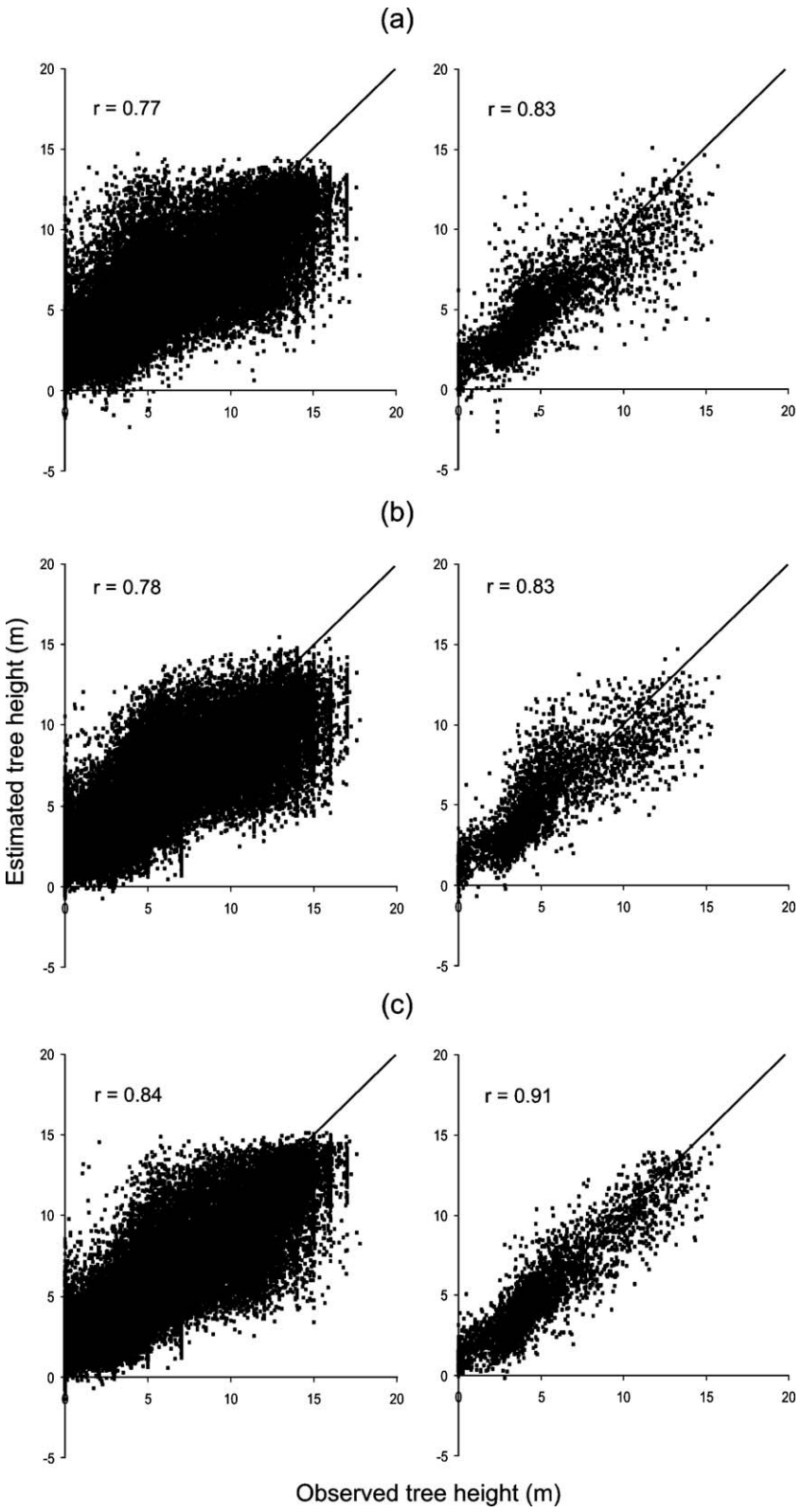

Fig. 8. Estimated versus observed tree height (m). See Fig. 7 for details.

spectral–angular data were used. The smallest RMSE ($RMSE_r$) was 4.06% (36.9%) for tree cover and 1.29 m (25.4%) for tree height, both predicted by all the 32 bands. Similar to the 275 m data, the division of the tree cover into the coniferous and broadleaved tree cover decreased RMSE (2.23% and 3.96%) but increased $RMSE_r$ (68.9% and 52.6%). The biases of the most accurate estimates were small and insignificant at 1.1 km resolution.

The multiangular data produced more accurate estimates than single nadir bands. At 275 m resolution, those bands

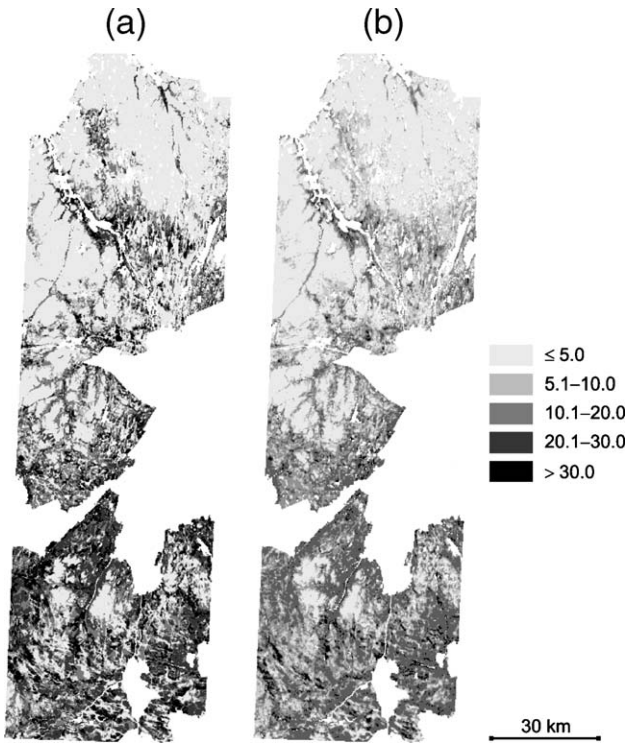

Fig. 9. Observed (a) and estimated (b) tree cover (%) at 275 m resolution. The tree cover was estimated using nadir and multiangular red bands.

produced also more accurate estimates than multispectral nadir data for all the target variables except coniferous tree cover. At 1.1 km resolution, the multiangular red data were the best predictor of tree cover, but the green data were the best predictor of tree height. The multispectral nadir data produced more accurate estimates of tree cover and height than multiangular blue and NIR data. The multiangular NIR and green data were more accurate predictor of the coniferous tree cover than nadir bands, and multiangular red data better predictor of broadleaved tree cover than nadir bands.

The tree cover and height estimates are plotted against the observed values in Figs. 7 and 8. The scattering in the plots is relatively small at 1.1 km resolution in comparison to the 275 m resolution. Furthermore, the scattering is reduced when the combined nadir and multiangular data are used instead of either nadir or single band multiangular data. The tree cover is also underestimated in the largest tree cover values corresponding to the slightly negative biases (Tables 2 and 3). Some underestimation also occurs in the tree height estimation, although the effect is smaller.

The observed and estimated tree cover has been mapped in Figs. 9 and 10, at 275 m and 1.1 km resolutions, and tree height in Figs. 11 and 12, respectively. The variables were estimated using all the spectral–angular data, because it produced the smallest estimation errors. The spatial patterns of observed and estimated tree cover and height are consistent, particularly at 1.1 km resolution. The largest underestimates of the tree cover and height occur in the areas of high tree cover, and in the coniferous forests in the southern part of the study area. The underestimation is particularly clear at 275 m resolution (Figs. 9 and 11). On the other hand, the tree cover and height are overestimated in the areas of low tree cover, particularly in the areas of dense shrub cover and in the mires. The overestimation occurs particularly in the middle and in the northern and parts of the study area.

3.3. Effect of shrub cover and mires to the estimation accuracy

The dependence of the estimation errors on shrub cover and fractional cover of mire was also examined. $RMSE_r$ and $Bias_r$ of the tree cover estimates are presented in relation to the shrub cover and fractional cover of mire in Figs. 13 and 14. At 275 m resolution, $RMSE_r$ of the tree cover increases as the shrub cover increases, but this is not observed at 1.1 km resolution. However, $Bias_r$ becomes larger as shrub cover increases. $RMSE_r$ and $Bias_r$ increase consistently when fractional cover of mire in the pixel becomes larger than 50%. The $Bias_r$ is also negative when shrub cover and fractional cover of mire are small. The same statistics are presented for tree height estimates in Figs. 15 and 16. $RMSE_r$ of the tree height estimates does not change or even reduce a little as shrub cover increases. Similarly to the tree cover estimates, $RMSE_r$ increase rapidly as the fractional cover of mire increase over 50% at 275 m resolution. However, $RMSE_r$ changes only a little between the classes at 1.1 km resolution. $Bias_r$ is negative when shrub cover and fractional cover of mire are small, but grows considerably as shrub cover and fractional cover of mire increase. However, the change in the $Bias_r$ is not as consistent as in the tree cover estimation.

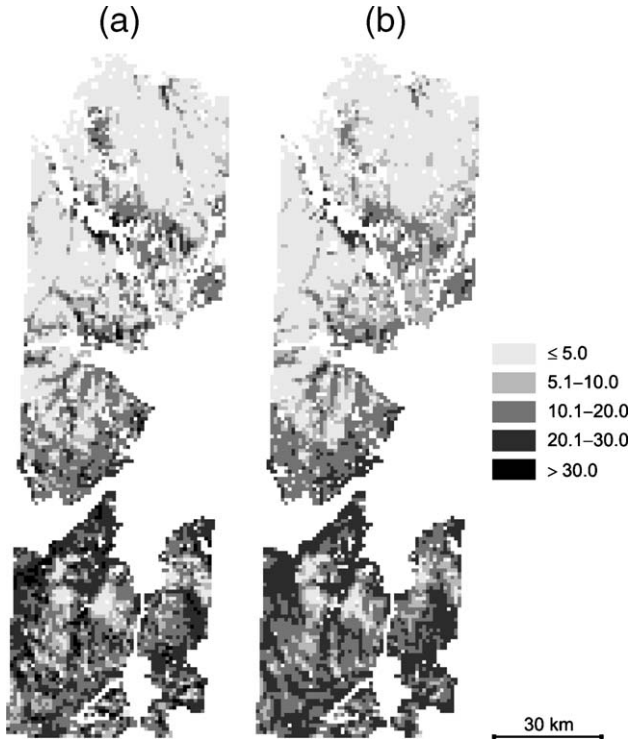

Fig. 10. Observed (a) and estimated (b) tree cover (%) at 1.1 km resolution. The tree cover was estimated using all the bands.

4. Discussion

The TOA and surface BRFs showed strong dependence on the view zenith angle (Figs. 5 and 6), although the view azimuth angles were approximately 20° off the solar principal plane (Fig. 3). The relationships are similar to those that have been reported for the azimuth angles off the solar principal plane (e.g., Deering et al., 1999; Russell et al., 1997). BRDF of forest canopies is typically characterised by strong reflectance in the backscatter direction with a peak in the hot spot. The directional dependence of the reflectance is usually weaker in the forward scatter direction, and reflectance reduces quickly as view azimuth angle increases off the principal plane (Bicheron et al., 1997; Deering et al., 1999; Kleman, 1987; Russell et al., 1997). The design and orbit of MISR does not allow observations closer to the principal plane, where BRDF effects are most pronounced (Chen et al., 2005). The slight increase of BRF in the largest view angles in the forward scatter direction was explained by Deering et al. (1999) by the high canopy transmission of broadleaved species and specular reflectance from the leaves. Furthermore, the atmospheric correction has a major effect on the directional reflectance because of path radiance and directional scattering of the atmosphere, particularly in the shortest wavelengths and largest view angles (Barnsley et al., 1997; Deering & Eck, 1987; Russell et al., 1997).

According to the mean BRFs of the tree cover and height classes, the red band seem to be the most sensitive band to the tree cover, and red and NIR bands the most sensitive bands to the tree height (Figs. 5 and 6). In the visible bands, the BRFs decrease as tree cover and height are increased because of higher absorption by the chlorophylls as leaf area increase. In the NIR, the reflectance is supposed to increase with increasing tree cover and height. However, the relatively large proportion of coniferous trees in the largest tree cover and height classes decreased the NIR reflectance, and the smallest and largest tree cover and height classes were confused.

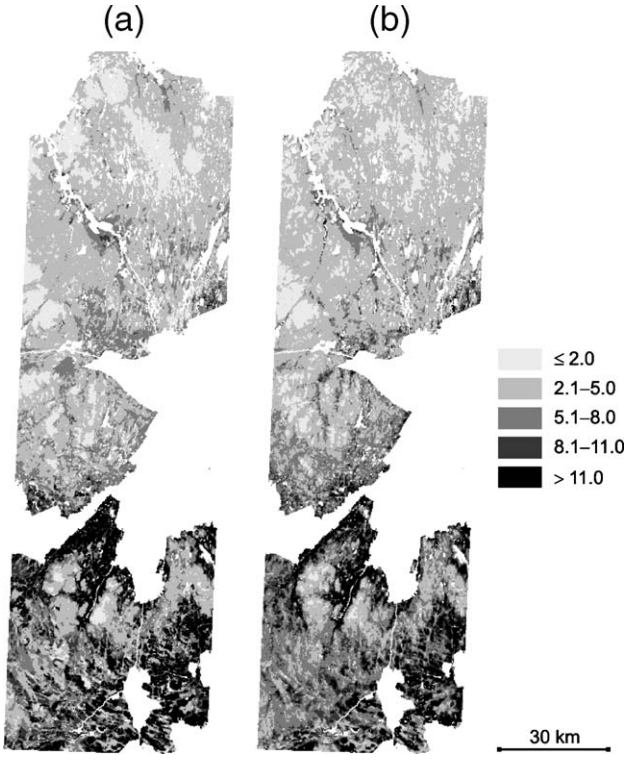

Fig. 11. Observed (a) and estimated (b) tree height (m) at 275 m resolution. The tree height was estimated using nadir and multiangular red bands.

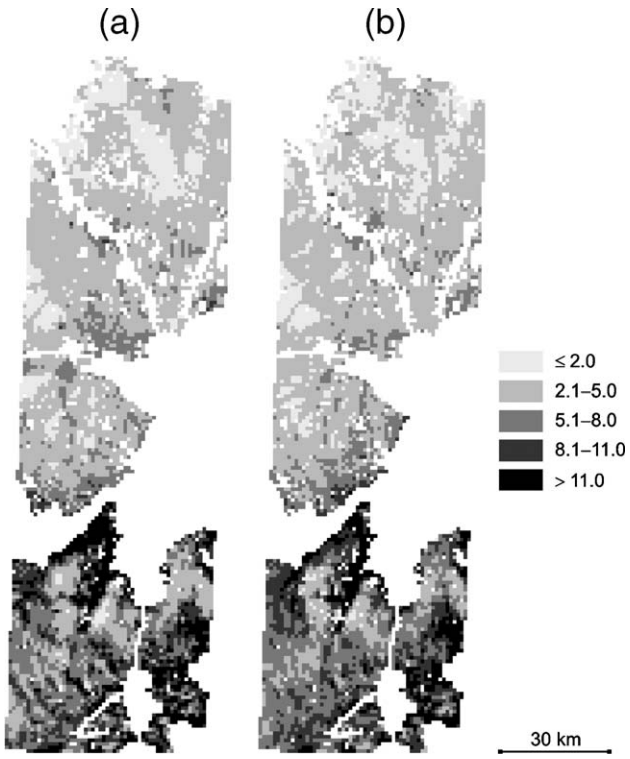

Fig. 12. Observed (a) and estimated (b) tree height (m) at 1.1 km resolution. The tree height was estimated using all the bands.

The most accurate estimates of all the target variables were achieved when using all the spectral–angular data. The multiangular data also produced more accurate estimates than the equivalent nadir bands. The potential of directional information to improve the discrimination of forest types and land cover classes have been demonstrated previously by several authors (Abuelgasim et al., 1996; Bicheron et al., 1997; Braswell et al., 2003; Sandmeier & Deering, 1999). Braswell et al. (2003) estimated sub-pixel land cover fractions in Brazilian Amazonia using MISR data, and got better model fit and lower estimation errors when using all the MISR bands as opposed to nadir data. Ranson et al. (2004) found that MISR red band data could produce consistent tundra–taiga transition zone maps with several other remote sensing data sets at several spatial resolutions. Gemmel (2000) concluded that multiangular data reduce the effects of background spectral variations in forest reflectance model inversion and hence improve the accuracy of the derived forest characteristics.

The tree cover and height were overestimated in the areas of dense shrub cover and in the mires, but overestimation was reduced to some extent when nadir data were coupled with multiangular data. Sandmeier and Deering (1999) found that the combination of nadir and off-nadir data improved substantially

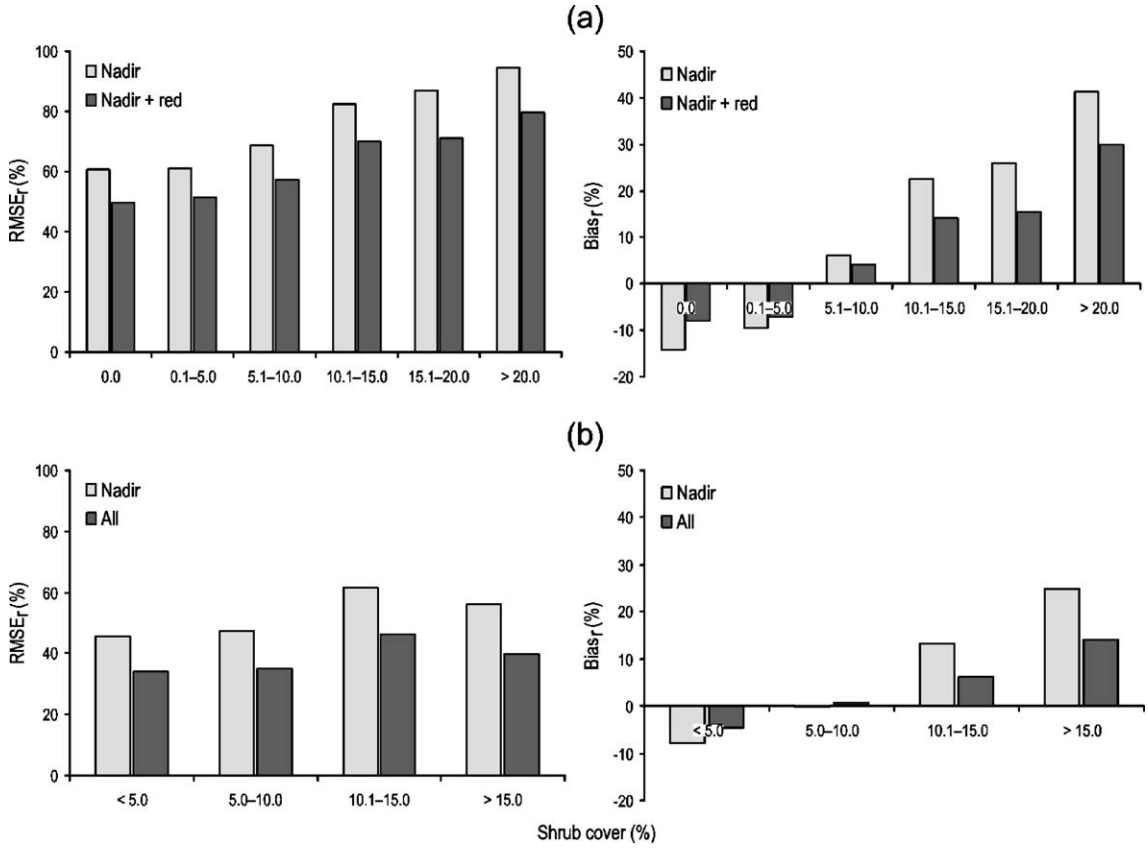

Fig. 13. The effect of shrub cover on the relative RMSE (on the left) and relative bias (on the right) of the tree cover estimates. (a) shows the accuracy at 275 m resolution and (b) at 1.1 km resolution.

the classification accuracy of the fen site. The conclusion was that multiangular data depend more on the canopy characteristics than on the undergrowth vegetation. Furthermore, the angular signature of inundated areas has been reported to be different from that of forests (Bicheron et al., 1997; Vanderbilt et al., 2002). The relatively strong forward scatter of mires is suggested by their bluish tone in the multiangular composite (Fig. 4b). However, the further examination of the angular signatures of the different land cover types was outside the scope of this study.

The smallest $RMSE_r$ were 56.1% and 37.6% for tree cover and tree height at 275 m resolution, and 36.9% and 25.4% at 1.1 km resolution, respectively. The estimation errors were considerably larger when coniferous and broadleaved tree cover was estimated separately. The pixel-wise estimation accuracy of the forest inventory variables has been assessed only rarely at a low spatial resolution (Hansen et al., 2002), although the applicability of the data depend on its accuracy. Schwarz and Zimmermann (2005) used generalized linear models (GLM) and MODIS data at 500 m resolution to estimate tree cover over the European Alps. The lowest mean absolute error (MAE) was 9.1%. For comparison, the lowest MAE of the tree cover was 4.7% at 275 m resolution and 3.0% at 1.1 km resolution in this study. If MAE is normalized by the mean tree cover (compare to Eq. (2)), the error in tree cover was 36.4% in Schwarz and Zimmermann (2005), and 41.0% and 27.5% at 275 m and 1.1 km resolution in this study. Therefore, the accuracy of the tree cover and height estimates seems to be relatively good. The relatively poor estimation accuracy is typical for species-wise estimates of forest inventory variables (Hyvönen, 2002; Mäkelä & Pekkarinen, 2004).

The tree height estimates were more accurate than tree cover estimates regardless of the combination of input bands or resolution. This is explained by the larger standard deviation of tree cover. However, the visible to NIR data could also be more sensitive to variability in tree height than in tree cover. The combination of nadir and multiangular bands reduced the estimation errors of the both tree cover and height almost equally. In relation to the multispectral nadir data, the maximum reduction in RMSE was 17% in tree cover and 15% in height estimates at 275 m resolution, and 25% and 28% at 1.1 km resolution. The broadleaved tree cover was also estimated more accurately than coniferous tree cover. Broadleaved forests are more abundant in the study area and in the training data than coniferous forests. Therefore, the standard deviation of the broadleaved tree cover is smaller than that of coniferous tree cover, and estimates are more accurate.

The best predictor varied between the target variables in the statistical analysis. The tree cover and broadleaved tree cover were estimated most accurately by the multiangular red bands, and coniferous tree cover by the NIR bands. The green bands were the best input data in the tree height estimation, but the

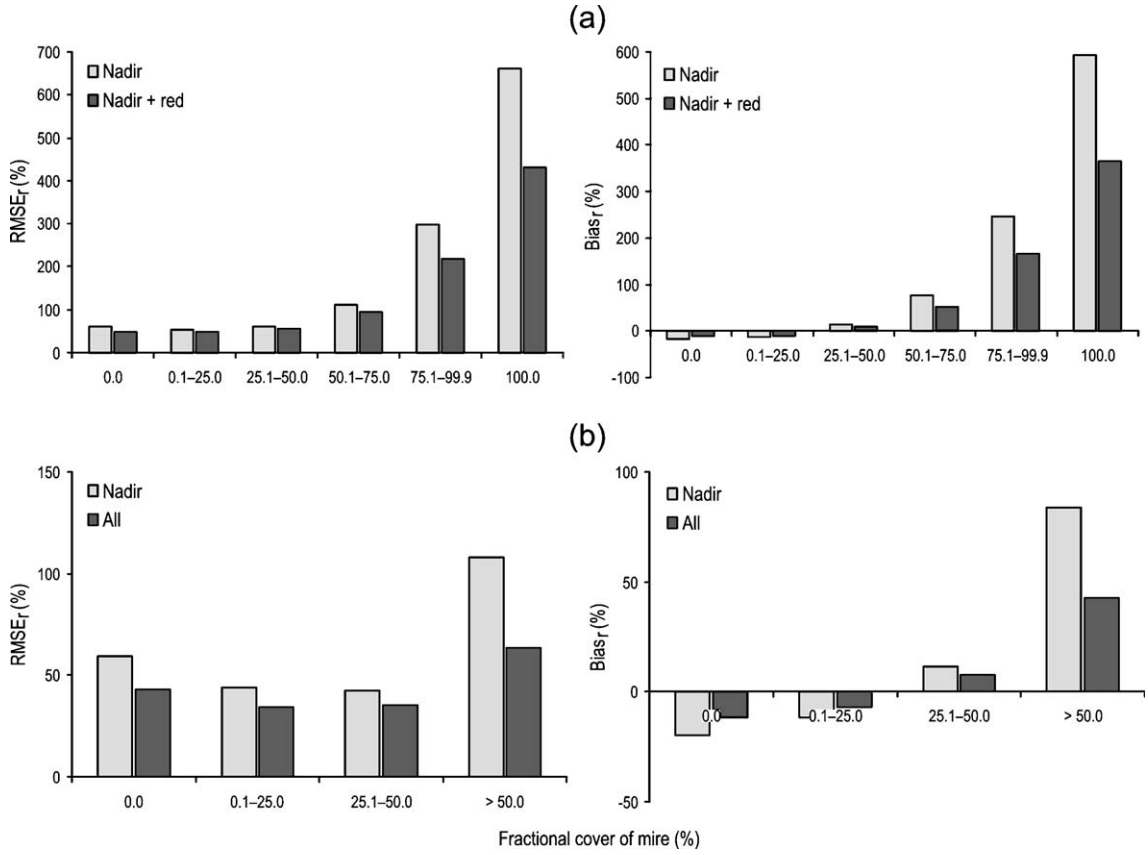

Fig. 14. The effect of mires on the relative RMSE (on the left) and relative bias (on the right) of the tree cover estimates. (a) shows the accuracy at 275 m resolution and (b) in the 1.1 km resolution.

difference with the red and NIR bands was very small. Table 3 showed that the estimation accuracy of tree cover and height is improved only a little when estimated using all the bands instead of the combination of the nadir and multiangular red bands. This is interesting since only multiangular red data is available at 275 m resolution in the MISR global mode. The improvement was the greatest in the case of coniferous tree cover, which was best estimated by using NIR bands.

The tree cover and height estimates were more accurate at 1.1 km than at 275 m resolution. The studies using high spatial resolution data to estimate forest variables, for example Landsat TM data, have shown that the estimation errors are improved as the inventoried area is increased. For example, per-pixel RMSE is typically around 60–80% for timber volume estimates at 30 m resolution, but the increase of inventory area to 30 ha can decrease the relative estimation error to approximately 20% (Mäkelä & Pekkarinen, 2004). Hansen et al. (2003) report that averaging of the percent tree cover product from 500 m to 1 km improved the validation measures dramatically. Similar results have been common (Hagen et al., 2002; Townshend et al., 2000).

The smaller standard deviation of the target variables at 1.1 km resolution is apparently one reason for better estimation accuracy at coarser resolution. However, the accuracy of the estimates is dependent also on the accuracy of the training data. The accuracy of the biotope inventory data used in this study have not been examined using independent field measurements, but Kunnari (2000) assessed the data against the interpretation keys collected in the field. The estimation errors were within the typical estimation error of the stand-wise forest inventory, which is around 20%. Only shrub cover estimates were significantly biased. The estimation errors in the biotope inventory data were reduced when up-scaling from 275 m resolution to 1.1 km resolution (Hansen et al., 2002). The bias in the shrub cover could be the reason for inconsistency, which was observed when estimation errors in tree height were studied in relation to shrub cover. The mires have been delineated accurately in the biotope inventory data (Kunnari, 2000), which could explain the better consistency of the results in relation to fraction cover of mire.

The scale of the estimation is not only limited by the spatial resolution of the satellite data but also by the scale of the training data. When relating field data to remotely sensed data, it is important that field data represent an area similar to the pixel of the image (Wulder, 1998). The mean size of the mapping units (tree covered) was 14.3 ha (median = 3.8 ha) in the biotope inventory data (n = 42656). The largest units were over 700 ha in size. Only 66% of the units were smaller than 275 m pixel (7.6 ha), but 98.2% of the units were smaller than 1.1 km pixels (121.0 ha). Hence, the biotope inventory could be better training data at 1.1 km resolution than at 275 m resolution, also partly explaining the better estimation accuracy at the lower resolution.

Quantitative interpretation of satellite data at the pixel level is hindered by the errors in the co-registration of training and

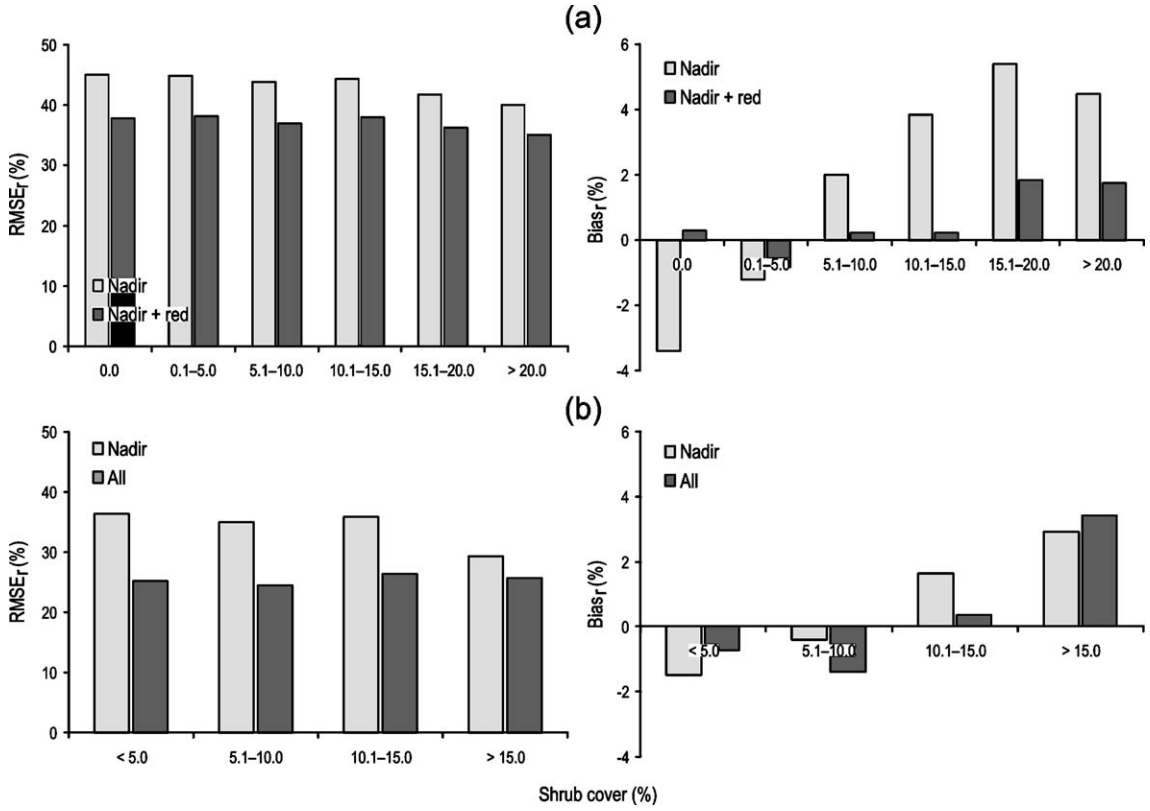

Fig. 15. The effect of the shrub cover on the relative RMSE (on the left) and relative bias (on the right) of the tree height estimates. (a) shows the accuracy at 275 m resolution and (b) at 1.1 km resolution.

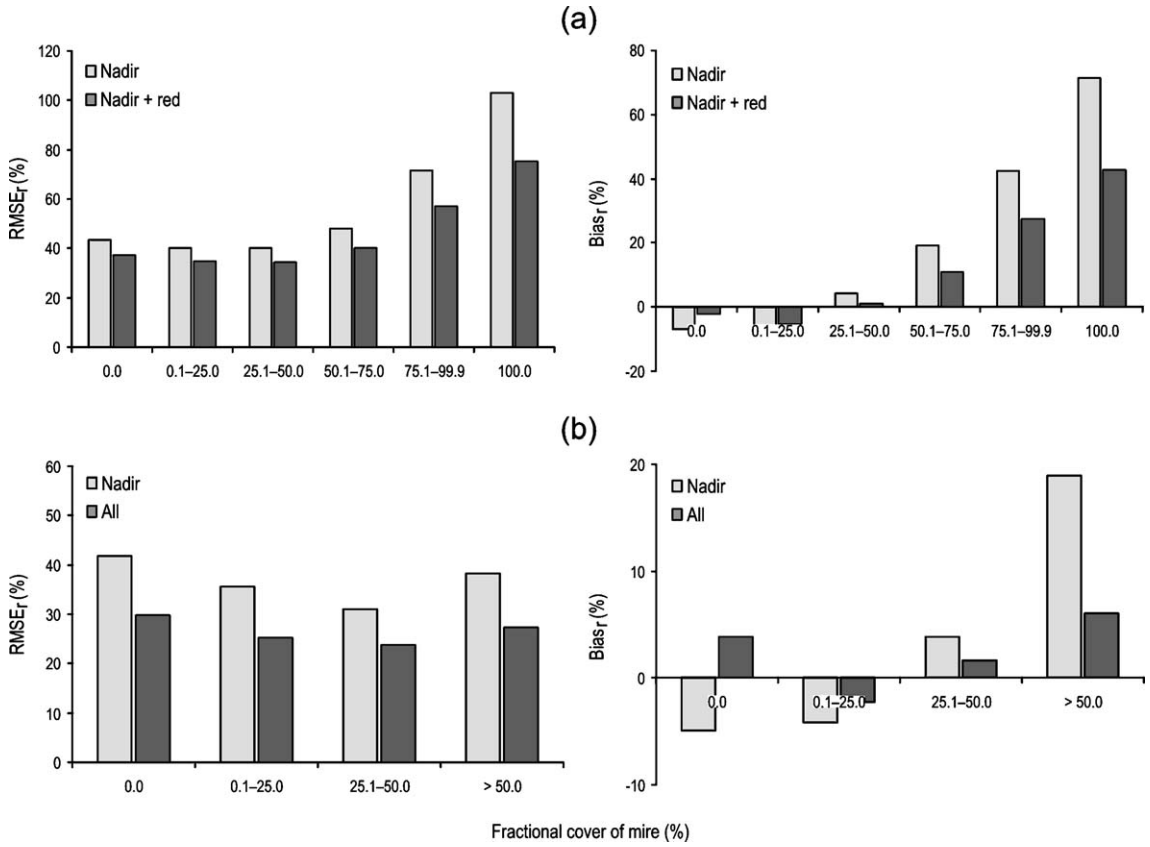

Fig. 16. The effect of mires on the relative RMSE (on the left) and relative bias (on the right) of the tree height estimates. (a) shows the accuracy at 275 m resolution and (b) at 1.1 km resolution.

satellite data. These errors are likely to be smaller at 1.1 km resolution than at 275 m resolution (Hagen et al., 2002). Furthermore, the averaging of the MISR data to 1.1 km resolution will reduce the adjacency effects (Huang et al., 2002; Townshend et al., 2000). Adjacency effects has been found to hinder the ability to derive surface information from satellite images on a per-pixel basis by decreasing the accuracy of the spectral mixture analysis (Townshend et al., 2000) and image classification (Huang et al., 2002). The off-nadir viewing, the lack of the atmospheric correction, and the bilinear interpolation used in the geometric correction (Jovanovic et al., 1998), are likely to pronounce the adjacency effects in the MISR data at 275 m resolution (Huang et al., 2002).

The effect of the atmospheric correction on the estimation accuracy could not be studied because of obvious artefacts in the MISR Level 2 Land Surface data. However, the differences between the tree cover and height classes were very similar in both TOA and surface data (Figs. 5 and 6), which suggest that atmospheric correction is unlikely to have a major effect on the estimation accuracy. This is also supported by Braswell et al. (2003), who found that the atmospheric correction did not affect the estimation accuracy of land cover fractions in the Brazilian Amazon. Furthermore, the topography also affects the multiangular data (Schaaf et al., 1994) and could lower the estimation accuracy. However, obvious topography related estimation errors were not observed when residuals of the estimates were mapped.

5. Conclusions

The comparison of different spectral–angular input combinations of MISR bands for tree cover and height estimation suggest that multiangular data and combination of multispectral and -angular data can provide improved tree cover and height estimates over visible to NIR nadir data for the heterogeneous tundra–taiga transition zone. The estimation accuracy was also improved somewhat in the shrub covered areas and mires, which have typically had the lowest classification accuracies in the study area. The results support the findings of the previous studies using multiangular data for land cover mapping. The multiangular data seem to increase sensitivity to the vegetation structure and reduce the effects of undergrowth vegetation which improves the estimation accuracy in comparison to nadir data. So far the use of multiangular data has been somewhat limited in land cover mapping (Braswell et al., 2003). Also, the use of sub-pixel estimation has been very limited in the tundra–taiga transition zone.

In this study, MISR data were used for testing the potential of multiangular data for tree cover and height estimation with extensive reference data. However, for mapping purposes, the atmospheric correction of satellite data and application of an appropriate BRDF model would be necessary. The BRDF model would be used for normalizing the observations to the same observation and illumination geometry, which would enable the combination of data from several orbits to cover larger areas. The atmospheric correction would enable also the collection of observations over a period of time to improve the BRDF characterization. After fitting a BRDF model to the observations, either BRDF model parameters (Lovell & Graetz, 2002) or some anisotropy index calculated from the model (Chen et al., 2005; Sandmeier & Deering, 1999) would be used for classification or estimation of land surface variables. The application of a BRDF model would also enable the separation of spectral and directional information (Barnsley et al., 1997; Hyman & Barnsley, 1997; Lovell & Graetz, 2002) for studying the relative importance of spectral and directional information in the land cover characterization.

Acknowledgements

The biotope inventory data were provided by Metsähallitus. MISR products were obtained from the Atmospheric Sciences Data Center (ASDC) at NASA Langley Research Center. The comments by Prof. Petri Pellikka, Mr. Barnaby Clark and anonymous referees were valuable to finish the manuscript.

References

Abuelgasim, A. A., Gopal, S., Irons, J. R., & Strahler, A. H. (1996). Classification of ASAS multiangle and multispectral measurements using artificial neural networks. *Remote Sensing of Environment*, *57*, 79–87.

Asner, G., Braswell, B., Schimel, D., & Wessmen, C. (1998). Ecological research needs from multiangle remote sensing data. *Remote Sensing of Environment*, *63*, 155–165.

Barnsley, M. J., Allison, D., & Lewis, P. (1997). On the information content of multiple view angle (MVA) images. *International Journal of Remote Sensing*, *18*, 1937–1960.

Bartalev, S. A., Belward, A. S., Erchov, D. V., & Isaev, A. S. (2003). A new SPOT4-VEGETATION derived land cover map of Northern Eurasia. *International Journal of Remote Sensing*, *24*, 1977–1982.

Bartholomé, E., & Belward, A. S. (2005). GLC2000: A new approach to global land cover mapping from Earth observation data. *International Journal of Remote Sensing*, *26*, 1959–1977.

Bicheron, P., Leroy, M., Hautecoeur, O., & Bréon, F. M. (1997). Enhanced discrimination of boreal forest covers with directional reflectances from the airborne polarization and directionality of Earth reflectances (POLDER) instrument. *Journal of Geophysical Research*, *102*(D24), 29517–29528.

Bishop, C. M. (1995). *Neural networks for pattern recognition.* New York: Oxford University Press. 482 pp.

Bothwell, G. W., Hansen, E. G., Vargo, R. E., & Miller, K. C. (2002). The Multi-angle Imaging SpectroRadiometer science data system, its products, tools, and performance. *IEEE Transactions on Geoscience and Remote Sensing*, *40*, 1467–1476.

Boyd, D. S., Foody, G. M., & Ripple, W. J. (2002). Evaluation of approaches for forest cover estimation in the Pacific Northwest, USA, using remote sensing. *Applied Geography*, *22*, 375–392.

Braswell, B. H., Hagen, S. C., Frolking, S. E., & Salas, W. A. (2003). A multivariable approach for mapping sub-pixel land cover distributions using MISR and MODIS: Application in the Brazilian Amazon region. *Remote Sensing of Environment*, *87*, 243–256.

Callaghan, T. V., Crawford, R. M. M., Eronen, M., Hofgaard, A., Payette, S., Rees, W. G., et al. (2002a). The dynamics of the tundra–taiga boundary: An overview and suggested coordinated and integrated approach to research. *Ambio Special Report*, *12*, 3–5.

Callaghan, T. V., Werkman, B. R., & Crawford, R. M. M. (2002b). The tundra–taiga interface and its dynamics: Concepts and applications. *Ambio Special Report*, *12*, 6–14.

Chen, J. M., Menges, C. H., & Leblanc, S. G. (2005). Global mapping of foliage index using multi-angular satellite data. *Remote Sensing of Environment*, *97*, 447–457.

Deering, D. W., & Eck, T. F. (1987). Atmospheric optical depth effects on angular anisotropy of plant canopy reflectance. *International Journal of Remote Sensing*, *8*, 893–916.

Deering, D. W., Eck, T. F., & Banerjee, B. (1999). Characterization of the reflectance anisotropy of three boreal forest canopies in spring–summer. *Remote Sensing of Environment*, *67*, 205–229.

DeFries, R. S., Hansen, M. C., & Townshend, J. R. G. (2000a). Global continuous fields of vegetation characteristics: A linear mixture model applied to multi-year 8 km AVHRR data. *International Journal of Remote Sensing*, *21*, 1389–1414.

DeFries, R. S., Hansen, M. C., Townshend, J. R. G., Janetos, A. C., & Loveland, T. R. (2000b). A new global 1-km dataset of percentage tree cover derived from remote sensing. *Global Change Biology*, *6*, 247–254.

DeFries, R. S., Townshend, J. R. G., & Hansen, M. C. (1999). Continuous fields of vegetation characteristics at the global scale at 1-km resolution. *Journal of Geophysical Research*, *104*, 16911–16923.

Diner, D. J., Asner, G. P., Davies, R., Knyazikhin, Y., Muller, J. -P., Nolin, A. W., et al. (1999). New directions in Earth observing: Scientific applications of multi-angle remote sensing. *Bulletin of the American Meteorological Society*, *80*, 2209–2228.

Diner, D. J., Beckert, J. C., Bothwell, G. W., & Rodriguez, J. I. (2002). Performance of the MISR instrument during its first 20 months in Earth orbit. *IEEE Transactions on Geoscience and Remote Sensing*, *40*, 1449–1466.

Diner, D. J., Beckert, J. C., Reilly, T. H., Bruegge, C. J., Conel, J. E., Kahn, R. A., et al. (1998). Multiangle Imaging SpectroRadiometer (MISR) instrument description and experiment overview. *IEEE Transactions on Geoscience and Remote Sensing*, *36*, 1072–1087.

Diner, D. J., Martonchik, J. V., Kahn, R. A., Pinty, B., Gobron, N., Nelson, D. L., et al. (2005). Using angular and spectral shape similarity constraints to improve MISR aerosol and surface retrievals over land. *Remote Sensing of Environment*, *94*, 155–171.

Eeronheimo, H., (ed., 1996). Metsähallituksen biotooppikuviointiohje. Kokeiluversio 16.5.1996. (47 pp.). Metsähallitus, Ylä-Lapin Luonnonhoitoalue, Ivalo (in Finnish).

Fernandes, R., Fraser, R., Latifovic, R., Cihlar, J., Beaubien, J., & Du, Y. (2004). Approaches to fractional land cover and continuous field mapping: A comparative assessment over the BOREAS study region. *Remote Sensing of Environment*, *89*, 234–251.

Gemmel, F. (2000). Testing the utility of multi-angle spectral data for reducing the effects of background spectral variations in forest reflectance model inversion. *Remote Sensing of Environment*, *72*, 46–63.

Hagen, S., Braswell, B. H., Frolking, S., Salas, W. A., & Xiao, X. (2002). Determination of subpixel fractions of nonforested area in the Amazon using multiresolution satellite sensor data. *Journal of Geophysical Research*, *107* (D20), 8049.

Häme, T., Salli, A., Andersson, K., & Lohi, A. (1997). A new methodology for the estimation of biomass of conifer-dominated boreal forest using NOAA AVHRR data. *International Journal of Remote Sensing*, *18*, 3211–3243.

Hansen, M. C., DeFries, R. S., Townshend, J. R. G., Carroll, M., Dimiceli, C., & Sohlberg, R. A. (2003). Global percent tree cover at a spatial resolution of 500 meters: First results of the MODIS vegetation continuous fields algorithm. *Earth Interactions*, *7*, 1–15.

Hansen, M. C., DeFries, R. S., Townshend, J. R. G., Marufu, L., & Sohlberg, R. A. (2002). Development of a MODIS tree cover validation data set for Western Province, Zambia. *Remote Sensing of Environment*, *83*, 320–335.

Hansen, M. C., DeFries, R. S., Townshend, J. R. G., & Sohlberg, R. (2000). Global land cover classification at 1 km spatial resolution using a classification tree approach. *International Journal of Remote Sensing*, *21*, 1331–1364.

Hansen, M. C., & Reed, B. (2000). A comparison of the IGBP DISCover and University of Maryland 1 km global land cover products. *International Journal of Remote Sensing*, *21*, 1365–1373.

Harding, R., Kuhry, P., Christensen, T. R., Sykes, M. T., Dankers, R., & van der Linden, S. (2002). Climate feedbacks at the tundra–taiga interface. *Ambio Special Report*, *12*, 47–55.

Heikkinen, O. (2005). Boreal forests and northern and upper timberlines. In M. Seppälä (Ed.), *The physical geography of Fennoscandia* (pp. 185–200). New York: Oxford University Press.

Huang, C., Townshend, J. R. G., Liang, S., Kalluri, S. N. V., & DeFries, R. S. (2002). Impact of sensor's point spread function on land cover characterization: Assessment and deconvolution. *Remote Sensing of Environment*, *80*, 203–212.

Hyman, A. H., & Barnsley, M. J. (1997). On the potential for land cover mapping from multiple-view-angle (MVA) remotely-sensed images. *International Journal of Remote Sensing*, *18*, 2471–2475.

Hyvönen, P. (2002). Kuvioittaisten puustotunnusten ja toimenpide-ehdotusten estimointi *k*-lähimmän naapurin menetelmällä Landsat TM-satelliittikuvan, vanhan inventointitiedon ja kuviotason tukiaineiston avulla. *Metsätieteen Aikakauskirja*, *3*, 363–379 (in Finnish).

Jovanovic, V. M., Bull, M. A., Smyth, M. M., & Zong, J. (2002). MISR in-flight camera geometric model calibration and georectification performance. *IEEE Transactions on Geoscience and Remote Sensing*, *40*, 1512–1519.

Jovanovic, V. M., Smyth, M. M., Zong, J., Ando, R., & Bothwell, G. W. (1998). MISR photogrammetric data reduction for geophysical retrievals. *IEEE Transactions on Geoscience and Remote Sensing*, *36*, 1290–1301.

Kalliola, R., & Syrjänen, K. (1991). To what extent are vegetation types visible in satellite imagery? *Annales Botanici Fennici*, *28*, 45–57.

Käyhkö, J., & Pellikka, P. (1994). Remote sensing of the impact of reindeer grazing on vegetation in northern Fennoscandia using SPOT XS data. *Polar Research*, *13*, 115–124.

Kleman, J. (1987). Directional reflectance factor distributions for two forest canopies. *Remote Sensing of Environment*, *23*, 83–96.

Kunnari, J. (2000). Metsähallituksen Ylä-Lapin luonnonhoitoalueen ja Urho Kekkosen kansallispuiston luontokartoitus: menetelmän luotettavuus. (33 pp.). Masters thesis, Forest planning and economics, University of Joensuu (in Finnish).

Loveland, T. R., Reed, B. C., Brown, J. F., Ohlen, D. O., Zhu, Z., Yang, L., et al. (2000). Development of a global land cover characteristics database and IGBP DISCover from 1 km AVHRR data. *International Journal of Remote Sensing*, *21*, 1303–1330.

Lovell, J. L., & Graetz, R. D. (2002). Analysis of POLDER-ADEOS data for the Australian continent: The relationship between BRDF and vegetation structure. *International Journal of Remote Sensing*, *23*, 2767–2796.

Mäkelä, H., & Pekkarinen, A. (2004). Estimation of forest stand volumes by Landsat TM imagery and stand-level field-inventory data. *Forest Ecology and Management*, *196*, 245–255.

Oksanen, L., & Virtanen, R. (1995). Topographic, altitudinal and regional patterns in continental and suboceanic heath vegetation of northern Fennoscandia. *Acta Botanica Fennica*, *153*, 1–80.

Ranson, K. J., Sun, G., Kharuk, V. I., & Kovacks, K. (2004). Assessing tundra–taiga boundary with multi-sensor satellite data. *Remote Sensing of Environment*, *93*, 283–295.

Rees, G., Brown, I., Mikkola, K., Virtanen, T., & Werkman, B. (2002). How can the dynamics of the tundra–taiga boundary be monitored? *Ambio Special Report*, *12*, 56–62.

Russell, C. A., Irons, J. R., & Dabney, P. W. (1997). Bidirectional reflectance of selected BOREAS sites from multiangle airborne data. *Journal of Geophysical Research*, *102*(D24), 29505–29516.

Ruuhijärvi, R. (1988). Suokasvillisuus. In P. Alalammi (Ed.), *Atlas of Finland, folio 141–143, biogeography, nature conservation* (pp. 2–6). Helsinki: National Board of Survey, Geographical society of Finland (in Finnish).

Sandmeier, S. T., & Deering, D. W. (1999). Structure analysis and classification of boreal forests using airborne hyperspectral BRDF data from ASAS. *Remote Sensing of Environment*, *69*, 281–295.

Schaaf, C. B., Li, X., & Strahler, A. H. (1994). Topographic effects on bidirectional and hemispherical reflectances calculated with a geometric-optical canopy model. *IEEE Transactions on Geoscience and Remote Sensing*, *32*, 1186–1193.

Schwarz, M., & Zimmermann, N. E. (2005). A new GLM-based method for mapping tree cover continuous fields using regional MODIS reflectance data. *Remote Sensing of Environment*, *95*, 428–443.

Seppälä, M., & Rastas, J. (1980). Vegetation map of northernmost Finland with special reference to subarctic forest limits and natural hazards. *Fennia*, *158*, 41–61.

Sihvo, J. (2001). Ylä-Lapin luonnonhoitoalueen ja Urho Kekkosen kansallispuiston luontokartoitus. Loppuraportti osa: 1. Projektikuvaus. *Metsähallituksen luonnonsuojelujulkaisuja*, *vol. A130*. 76 pp. (in Finnish).

Sihvo, J. (2002). Ylä-Lapin luonnonhoitoalueen ja Urho Kekkosen kansallispuiston luontokartoitus. Loppuraportti osa: 2. Ylä-Lapin luontotyypit. *Metsähallituksen luonnonsuojelujulkaisuja*, *vol. A137*. 175 pp. (in Finnish).

Skre, O., Baxter, R., Crawford, R. M. M., Callaghan, T. V., & Fedorkov, A. (2002). How will the tundra–taiga interface respond to climate change. *Ambio Special Report*, *12*, 37–46.

Stow, D. A., Hope, A., McGuire, D., Verbyla, D., Gamon, J., Huemmrich, F., et al. (2004). Remote sensing of vegetation and land-cover change in Arctic tundra ecosystems. *Remote Sensing of Environment*, *89*, 281–308.

Tomppo, E., Nilson, M., Rosenberg, M., Aalto, P., & Kennedy, P. (2002). Simultaneous use of Landsat-TM and IRS-1C WiFS data in estimating large area tree stem volume and aboveground biomass. *Remote Sensing of Environment*, *82*, 156–171.

Townshend, J., Huang, C., Kalluri, S., DeFries, R., Liang, S., & Yang, K. (2000). Beware of perpixel characterization of land cover. *International Journal of Remote Sensing*, *21*, 839–843.

Vanderbilt, V. C., Perry, G. L., Livingston, G. P., Ustin, S. L., Diaz Barrios, M. C., Bréon, F. M., et al. (2002). Inundation discriminated using sun glint. *IEEE Transactions on Geoscience and Remote Sensing*, *40*, 1279–1286.

Virtanen, T., Mikkola, K., & Nikula, A. (2004). Satellite image based vegetation classification of a large area using limited ground reference data: A case study in the Usa Basin, north–east European Russia. *Polar Research*, *23*, 51–66.

Vlassova, T. K. (2002). Human impacts on the tundra–taiga zone dynamics: The case of the Russian lesotundra. *Ambio Special Report*, *12*, 30–36.

Wulder, M. (1998). Optical remote-sensing techniques for the assessment of forest inventory and biophysical parameters. *Progress in Physical Geography*, *22*, 449–476.